buildings

MDPI

Article

Low-Field Nuclear Magnetic Resonance Investigation on Early Hydration Characterization of Cement Paste Mixed with Mineral Admixtures

Yu-Juan Tang [1], Zi-Qi Shan [2], Guang-Ji Yin [2,*], Ling Miao [3], Sai-Sai Wang [2] and Zhen-Ya Zhang [2]

[1] School of Civil and Engineering, Yangzhou Polytechnic College, Yangzhou 225009, China; tyjdsr19891103@163.com
[2] School of Civil and Transportation Engineering, Ningbo University of Technology, Ningbo 315211, China; shanziqi1013@163.com (Z.-Q.S.); wss@nbut.edu.cn (S.-S.W.); zhangzhenya@nbut.edu.cn (Z.-Y.Z.)
[3] College of Art and Design, Nanjing Forestry University, Nanjing 210037, China; miaoling@njfu.edu.cn
* Correspondence: yinxjlove@163.com

Abstract: Mineral admixtures (MA), like fly ash (FA), silica fume (SF), and slag (S), are usually added to cement-based materials to improve their compactness and further enhance their mechanical properties, permeability resistance, and durability. In this study, low-field nuclear magnetic resonance (LF-NMR) is adopted to explore the evolution of the early hydration characterization of cement-based materials with MA by testing the transverse relaxation time T2. Meanwhile, the effect of MA on mechanical properties is analyzed by measuring compressive and flexural strength. The results show that, in the early hydration (0–7 days), the T2 distribution shows a trend of gradually moving to a short relaxation time and changes from a double peak to a single main peak. The decrease in T2i (main peak vertex) means that the evaporated water is gradually distributed in smaller pores with more motion constraints. However, the type and content of MA have little effect on T2i. Porosity gradually decreases in the period of early hydration. The addition of MA causes the porosity to decrease, and the order influence is FA > S > SF, i.e., the porosities of cement paste with 0%MA, 10%FA + 10%SF, 10%FA + 10%S, and 20%FA at 7 days are 48%, 44.5%, 40.7%, and 40.2%, respectively. Additionally, the addition of MA to cement-based materials also decreases the early strength, and the influence order is FA > S > SF, i.e., the compression strength values of cement paste with 0%MA, 10%FA + 10%SF, 10%FA + 10%S, and 20%FA at 7 days are 47.8 MPa, 40.1 MPa, 38.6 MPa, and 37 MPa, respectively.

Keywords: hydration characterization; low-field nuclear magnetic resonance; transverse relaxation time; porosity of cement paste

check for updates

Citation: Tang, Y.-J.; Shan, Z.-Q.; Yin, G.-J.; Miao, L.; Wang, S.-S.; Zhang, Z.-Y. Low-Field Nuclear Magnetic Resonance Investigation on Early Hydration Characterization of Cement Paste Mixed with Mineral Admixtures. *Buildings* **2023**, *13*, 2318. https://doi.org/10.3390/buildings13092318

Academic Editor: Yunchao Tang

Received: 23 August 2023
Revised: 7 September 2023
Accepted: 11 September 2023
Published: 12 September 2023

Copyright: © 2023 by the authors. Licensee MDPI, Basel, Switzerland. This article is an open access article distributed under the terms and conditions of the Creative Commons Attribution (CC BY) license (https://creativecommons.org/licenses/by/4.0/).

1. Introduction

Concrete is one of the most widely used building materials in the world today. Its transition from a plastic flow state to a hardened brittle state is mainly attributed to the cement hydration reaction [1]. When the cement is mixed with water, it undergoes vigorous hydration reactions to produce C-S-H gel (semi-crystalline and amorphous hydrated calcium silicate, the detailed description of which can be found in references [2,3]), CH crystals (hexagonal crystal system), and other hydration products. As the hydration products increase, the gel particles agglomerate into a network structure, causing the cement paste to thicken and gradually lose its plasticity, i.e., setting behavior. Subsequently, the hydration products continue to fill the space between cement particles, causing the paste to gradually densify and harden [4], i.e., hardening behavior. At this stage, the mechanical property of cement paste develops rapidly. In summary, during the process of cement hydration, the cement paste undergoes a drastic evolution of microphase, morphology and pore structure, ultimately hardening into a heterogeneous porous material. Therefore, the hydration behavior of cement plays a crucial role in the flowability, mechanical properties, and durability of cement-based materials [5].

For ordinary Portland cement, the main reason for its long-term service performance is the presence of the surface defects of the hardened matrix and its non-dense internal structure. The addition of MAs, such as fly ash (FA) [6], slag (S) [7], and silica fume (SF) [8], to cement-based materials can improve their various performances. Due to the low pozzolanic effect of FA, the reaction rate between FA and CH of cement hydration products is very slow within 7 days of hydration [9]. It reduces the hydration process of the FA-C (cement) system, resulting in low early mechanical properties [10]. With the excitation of the pozzolanic effect, the mechanical properties of the FA-C system are gradually improved. Generally speaking, after 90 days of hydration, the reaction of FA with CH has not yet ended. In addition, FA also has morphological and microaggregate effects, which can improve the workability of the FA-C system [11]. Small particles of FA (with an average particle size of 15–20 mm) can effectively fill the pores between hydration products, improving the structural density of cement-based materials [12]. For the silica fume (SF), the content of active SiO_2 is high (>80%). When SF is added to cement, it can react earlier with CH formed by the cement hydration to generate C-S-H gel, i.e., giving better play to the pozzolanic effect [13,14]. Meanwhile, microparticles of SF (with a particle size of about 100 nm) can effectively fill the large pores in the interfacial transition zone between cement paste and aggregate [14]. It improves the structural density of the SF-C system and causes its early compressive strength. Similar to FA, slag (S) also has the pozzolanic and microaggregate effect [5]. So, the influence of its addition to cement on the hydration progress, pore structure, and early strength of the S-C system is also similar to that of FA. In summary, MAs can significantly improve the microstructure of cement-based materials, further increase their later mechanical properties (28 days) and permeability resistance, and significantly inhibit the alkali–aggregate reaction [15,16]. In response to the problems of low early strength and shrinkage cracking, the main method is to mix multiple MAs into cement. At present, the research on the effect of multiple MA addition is very rich, i.e., the synergistic effect of FA and ground granulated blast furnace slag (GGBFS) [17,18], FA and ferrochrome slag [19], F-class FA and nano-SF [20,21], FA, palm oil fuel ash and GBFS [22], SF and metakaolin [23], SF and GGBFS [24], SF and rice husk ash [25,26], SF and glass powder [27], and SF and ferrosilicon [28] on the microstructure and mechanical properties like strength and shrinkage of cement-based materials. By superimposing the regulating effects of MAs on the behavior of cement hydration, the overall performance of cement-based materials can be improved.

The traditional testing methods for cement hydration behavior mainly include the isothermal calorimetry method [29,30], the chemically bound water method [31], and the CH quantitative analysis method [32]. Based on the heat release curve measured by isothermal calorimetry, the process of cement hydration is divided into five stages, i.e., the dissolution, induction, acceleration, deceleration, and stabilization stages. However, Scrivener [33] divided the hydration process into three stages, including the stage before induction end, the main hydration front stage, and the slow reaction stage. According to the measured data of hydration heat, the basic parameters in the model of cement hydration reaction kinetics (such as the Krstulović–Dabić model [34]) can be determined. So, a kinetics equation of hydration degree related to reaction time can be established. However, the isothermal calorimetry is not suitable for analyzing the hydration behavior of cement-based materials with MAs [35,36], because their influence on the cement hydration heat has not been quantified. The chemically bound water method is a method of determining the content of chemically bound water in cement hydration products by the calcination form, to deduce its hydration degree. However, for cement-based composite systems, this method cannot distinguish whether the bound water comes from the hydration of cement or MAs. In summary, traditional testing methods have effectively revealed the process of cement hydration but cannot quantify the impact of MA on the cement hydration. With the development of non-destructive testing technology, methods such as electrodeless resistivity testing [37], dielectric constant testing, and ultrasonic velocity testing [38,39] have been applied to the analysis of the hydration behavior of cement-MA system hydration.

Electrical resistivity can reflect the porosity evolution of cement paste in the process of setting and hardening. Li et al. [40] combined electrodeless resistivity and ultrasonic velocity testing to analyze the cement hydration behavior, proving that both methods are effective for continuous monitoring.

The hydration reaction of cement is often accompanied by the transition behavior of the water state in addition to the heat release and the microstructural changes in cement paste. During the hydration process, free water gradually transforms into chemically bound water, physically adsorbed water, and pore water [41], resulting in volume shrinkage, micropore formation, and strength increase in concrete. In recent years, the relaxation method of nuclear magnetic resonance (NMR) has been increasingly developed and applied to analyze the changes in water state caused by cement hydration reactions [42,43]. In the relaxation method, the spin–lattice relaxation time T_1 and spin relaxation time T_2 are mainly used to describe the response of ^{1}H nucleus spin magnetization to resonance excitation. Compared to T_1, the signal value of T_2 decreases as the mobility of water molecules decreases (the movement of water molecules is limited by their space) [44], which can better characterize the different states of water [45]. Using the one-dimensional frequency coding technology of low-field (LF) NMR, Zhao et al. [46] analyzed the transport behavior of liquid water in cement-based materials with different mix proportions (water–cement ratio, sand–cement ratio, silica fume content, etc.). Zhang et al. [47] continuously tested the transverse relaxation time T_2 in the hydration process of white cement with SiO_2 nanoparticles to analyze the influence of SiO_2 particle size on the hydration reaction, and then determined the setting time. According to the relaxation time T_2, Liu et al. [48] divided the hydration behavior into the heating, thermostatic, and colling processes and established a mathematical model for the relation between T_2 and the hydration degree. It should be pointed out that most of the NMR studies [46–49] used white cement with a low content of Fe_2O_3 as the material to reduce the impact of iron on the NMR signal. However, recent reports [50,51] have adopted ordinary Portland cement as the research material, and the results in [51] explain well the relationship between pore structure and capillary water in cement-based materials.

In a word, besides the isothermal calorimetry method, the relaxation method of nuclear magnetic resonance (NMR) is also an effective method to analyze the hydration of cement paste. The transverse relaxation time T_2 can reflect the motility of water molecules constrained by their space, i.e., the pore structure for cement-based materials. In this paper, LF-NMR is adopted to measure the T_2 signal of cement-based materials with FA, SF, and S. According to the relationship between T_2 (its value, area, and peak signal) and water motility, the effect of MA type and content on the early hydration characterization (pore structure, water state) can be further analyzed, especially during the first 24 h of hydration. Meanwhile, the compressive and flexural strength of cement paste with different MA is tested at the early hydration stage. On this basis, the collaborative analysis of the evolution of pore structure and the development of mechanical properties can help to better understand the regulatory effect of composite admixtures.

2. Testing Principle

Based on Brownstein–Tarr's model (BT model) [52], the transverse relaxation time T_2 of moisture in cement-based materials can be expressed as

$$\frac{1}{T_2} = \frac{1}{T_{2S}} + \frac{1}{T_{2D}} + \frac{1}{T_{2B}},\ \frac{1}{T_{2S}} = \rho_2 \frac{S}{V},\ \frac{1}{T_{2D}} = \frac{D_w}{12}(\gamma G T_E)^2 \quad (1)$$

where T_{2S} is the particle surface relaxation time, T_{2D} is the molecular diffusion relaxation time, T_{2B} is the water-free relaxation time, ρ_2 is the transverse surface relaxation strength, S and V are the specific surface area and volume of pores, D_w is the diffusion coefficient of water molecules, G is the gradient of the external magnetic field, and T_E is the echo time.

Due to the value of T_{2B} being approximately 2–3 s, which is much greater than the transverse relaxation time T_2 [45], T_{2B} in Equation (1) can be ignored. For a uniform

external magnetic field, its gradient G is extremely small and the echo interval is short, and T_{2D} in Equation (1) can also be ignored. Therefore, the T_2 is mainly determined by the surface relaxation time of particles [53], which can be simplified as

$$\frac{1}{T_2} \approx \frac{1}{T_{2S}} = \rho_2 \frac{S}{V} \tag{2}$$

in which S/V is equal to $3/r$ for spherical pores and $2/r$ for columnar pores, and r is the pore radius.

At present, T_2 is mainly measured by using the CPMG (Carr–Purcell–Meiboom–Gill) pulse sequence [54,55], as shown in Figure 1. Firstly, a 90° pulse is applied to deflect the magnetization vector to the x-y plane. Due to the non-uniformity of the applied magnetic field, the transverse components of the magnetization vector undergo phase dispersion. After the $T_E/2$ time, a 180° pulse is applied to reunite the phase-dispersed transverse components, and then an echo can be observed after the T_E time (the end of the 180° pulse). So, if a series of 180° pulses are continuously applied at intervals of T_E time, an echo string with continuous attenuation of signal amplitude can be obtained, and the envelope curve of this series of signal peaks represents a relaxation signal. By repeating the above testing process m times, the accumulated total relaxation signal can be obtained, and the attenuation law of signal amplitude meets Equation (3). Using InvFit inversion software, the total relaxation signal is processed to obtain the T_2 spectrum of moisture in porous cement-based materials.

$$M(t) = \sum_m M_{h0} \exp\left(-\frac{t}{T_2}\right) \tag{3}$$

where T_E is the echo time, and m is the repeated times.

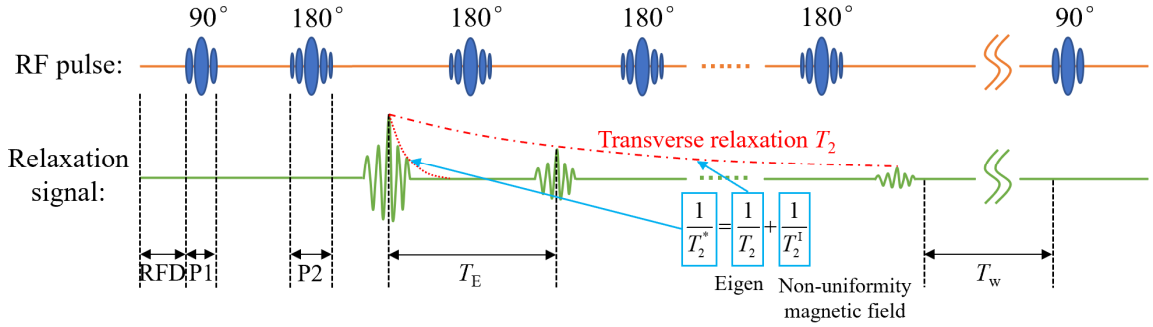


Figure 1. CPMG pulse sequence.

3. Experiment

3.1. Materials

The cement used in this study was 42.5-grade P·I cement, whose chemical composition is listed in Table 1, with a density of 3120 kg/m^3 and a specific surface area of 358 m^2/kg. The initial and final setting times are 115 min and 188 min, respectively, and its normal compression strength and flexural strength for 28 days of curing are 51.2 MPa and 8.8 MPa, respectively. Fly ash and slag are produced by China Longze Materials Co., Ltd., (Yang Zhou City, China) and their basic properties and chemical compositions are shown in Tables 2 and 3, respectively.

Table 1. Chemical composition of cement (%).

SiO_2	Al_2O_3	Fe_2O_3	CaO	MgO	SO_2	Na_2O	f-CaO	Cl^-	Loss
20	4/40	3.27	63.34	2.90	2.42	0.59	0.87	0.02	1.54

Table 2. Basic properties and chemical composition of fly ash.

Physical property	Fineness (45 mm Square Hole Sieve) (%)	Water Demand Ratio (%)	Strength Activity Index (%)	Water Content (%)	Density (g/cm^3)
	20	98	86	0.52	2.25
Chemical composition	SO_3 (%)	f-CaO (%)	SiO_2 (%)	Al_2O_3 (%)	Fe_2O_3 (%)
	2.16	0.26	50.26	31.14	4.16

Table 3. Basic properties and chemical composition of slag.

Physical property	Specific Surface Area (m^2/kg)		Flow Ratio (%)	7 Days Activity Index (%)	Water Content (%)	Density (g/cm^3)
	429		98	84.2	0.45	3.1
Chemical composition	SO_3 (%)	MgO (%)	CaO (%)	SiO_2 (%)	Al_2O_3 (%)	Fe_2O_3 (%)
	1.64	6.01	34	34.5	17.7	1.03

The mixed cement paste with a water–cement ratio of 0.4 was injected into the chromatographic bottles, slightly vibrated to eliminate air, and then sealed to prevent free water from evaporating, as shown in Figure 2. The mix proportion of cement paste is according to the "Specification for mix proportion design of ordinary concrete" (JGJ55-2011), as shown in Table 4. At room temperature, an NMR instrument was used to regularly measure the T_2 spectrum in the process of cement hydration.



Figure 2. Chromatographic bottle containing cement paste.

Table 4. Mix proportions of cement paste (mass proportion).

Number	W/C	Cementitious Material			
		Cement (C)	Fly ash (FA)	Slag (S)	Silica Fume (SF)
JJ-1	0.4	1	0	0	0
JJ-2	0.4	0.8	0.2	0	0
JJ-3	0.4	0.6	0.4	0	0
JJ-4	0.4	0.8	0.1	0.1	0
JJ-5	0.4	0.6	0.3	0.1	0
JJ-6	0.4	0.8	0.1	0	0.1
JJ-7	0.4	0.6	0.3	0	0.1

3.2. Measure Method

In cement-based materials, evaporable water can be divided into free water, physically adsorbed water, and chemically bound water, according to the motility of water

molecules [56]. In the process of cement hydration, the original water space is gradually filled with cement-hydrated products, while the unfilled water space forms capillary pores, and the water present in capillary pores is called free water. In the space filled by hydration products, the pores between hydration products are called transition pores, the pores between hydration products C-S-H gel particles are called gel pores, and the water in them is mainly physically adsorbed water. The chemically bound water refers to the water combined with C-S-H gel by hydration reaction, which cannot be evaporated. In summary, during the hydration process, the water changes from a free state to physically adsorbed and chemically bound state, with some remaining in the form of free water.

Based on the correlation between moisture state and hydration kinetics [57], this study analyzes the cement hydration characterization by testing the T_2 signals of ^{1}H nuclei in samples of cement-based materials. The LF-NMR experiments were performed using a MesoMR12-060H-1 NMR analysis and imaging system (Suzhou Niumag Analytical Instrument Corporation, Suzhou, China). The permanent magnet magnetic field strength is 0.5 T, the proton resonance frequency is 23 MHz, and the magnet is controlled at a constant temperature of 32 °C. Adjusting the instrument system parameters before the testing, the cement paste samples with different mix proportions were inserted into the instrument probe coil and measured by adopting the CPMG pulse sequence [54]. Its pulse widths of 90° and 180° pulses are 7.40 μs and 14.24 μs, respectively, the echo time is 100 μs, the echo number is 2000, and the accumulative frequency (m) is 32. The specific testing process is shown in Figure 3.



Figure 3. NMR instrument.

4. Result and Discussion

4.1. Distribution of Relaxation Time

Figure 4 shows the transverse relaxation time (T_2) of cement paste with different mix proportions at different curing times. The results show that, at the same curing time, the distribution of T_2 is similar for each mix proportion and presents an obvious main peak and a weak peak (or no weak peak). With the increase in curing time, the relaxation peak signal corresponding to large T_2 gradually decreases, while the peak signal corresponding to small T_2 gradually increases. The distribution of the relaxation peak shows a trend of gradually moving to a short relaxation time and gradually changing from a double peak to a single main peak [48]. In particular, the T_2 distribution of JJ-7 becomes a single peak at the curing time of 9 h, while those of other samples are still two peaks.

According to the NMR principle, T_{2i} (T_2 corresponding to the main peak vertex) reflects the motion characteristics of water molecules [58]. For the liquid water, the stronger its motion ability and the less its motion constraints, the larger its T_{2i}. Figure 5 presents the change in T_{2i} for different cement paste with curing time. It is obvious that T_{2i} has a rapid decrease at the early hydration age (within 24 h) and then gradually stabilizes. The

main reason for the above phenomena is that the relaxation time of confined fluid water in a porous medium is inversely proportional to the specific surface area of its pore [59]. In the curing process, the hydration products continuously generate to fill and refine the larger pores [15,60], causing the unreacted evaporated water to be gradually distributed in smaller pores with more motion constraints. So, the T_{2i} becomes small. In addition, the T_{2i} of JJ-1 (without MA) is larger than that of other samples. For the same curing time, the T_{2i} of cement paste with different MAs are basically the same. It means that the cement content has a slight influence on T_{2i} [61], while the type and content of MAs have little effect.

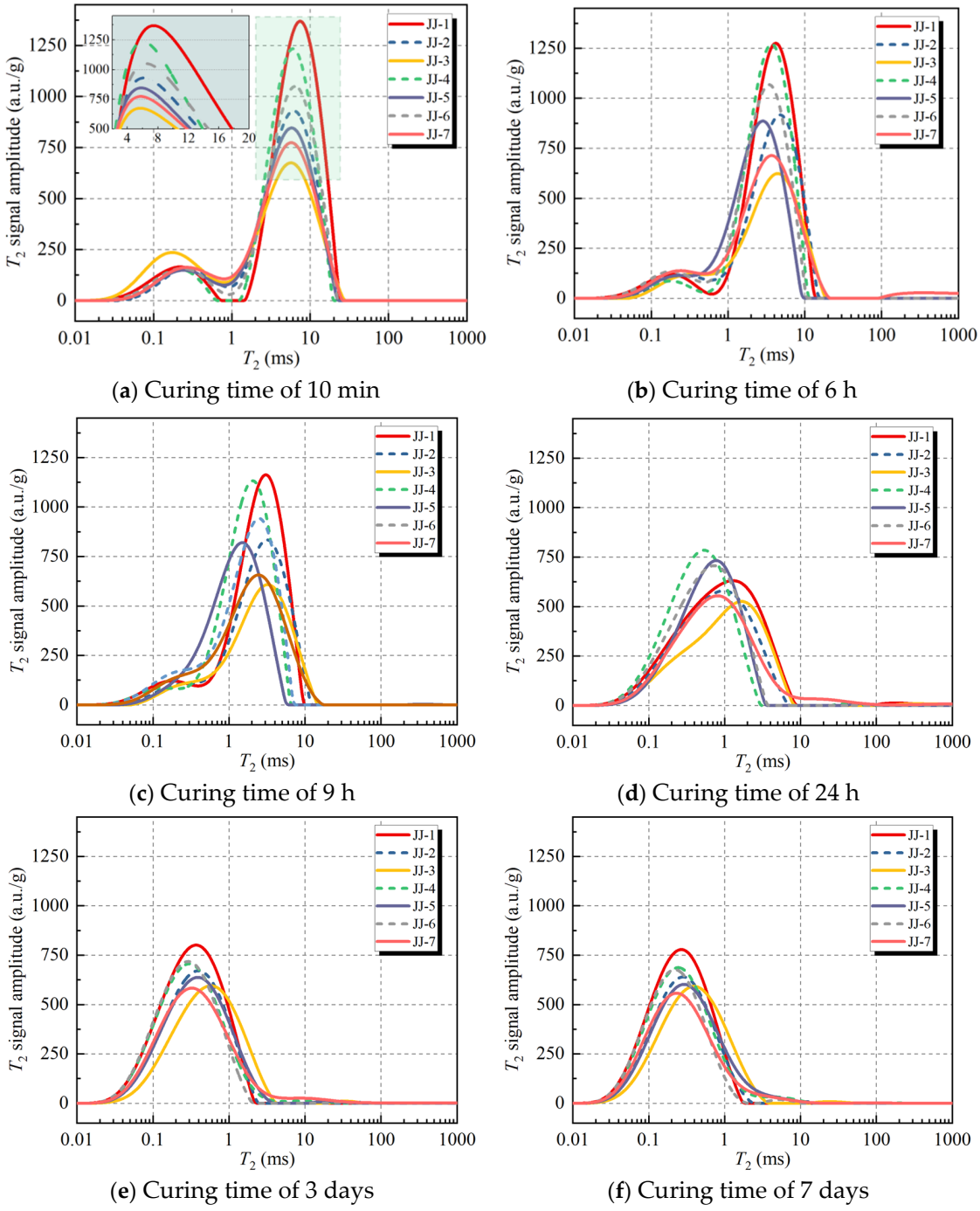


Figure 4. T_2 spectra of cement-based materials at different curing ages.

Besides the decrease in relaxation time, the change in relaxation signal for different samples can also be obtained from Figure 4. Especially at the curing age of 10 min, the

relaxation signal of the main peak vertex for JJ-1 is 1370.17, while that for JJ-3 (replacing 40% cement with FA) is 675.53. The signal difference between the two is almost 100%. At the curing age of 24 h, the vertex relaxation signals for JJ-1, JJ-3, and JJ-5 are 778.85, 592.59, and 558.00, respectively, and there is not much difference between them. So, the influence of MAs on the relaxation signal of the specimen is mainly reflected in the early stage of cement hydration.

The relaxation signal area is proportional to the number of ^{1}H protons in the samples, and the larger the signal area, the more water content the specimen contains [62]. Figure 6 presents the effect of MAs on the relaxation signal area of T_2 in the hydration time. It can be seen from this figure that the signal area shows a downward trend with the increase in hydration time. The decline rate is fast at the early stage, while the decline rate slows down later. Due to the same type and proportion of water and cement in samples, the smaller the signal area, the more water is consumed in the hydration reaction. It can be known from Figure 6a that the addition of FA accelerates the hydration behavior of cement, and the greater the FA content, the faster the cement hydration. It is because the low-activity FA rarely undergoes hydration reactions during short-term curing, so the addition of FA improves the effective water–cement ratio, accelerating the cement hydration. Certainly, this phenomenon does not contradict the fact that the addition of FA slows down the hydration progress of the FA-C system. Figure 6b,c show that replacing FA with S or SF slows down the hydration rate of the FA-S-C or FA-SF-C system. The reason is that the S and SF have certain activity and undergo hydration reactions in an alkaline environment formed by cement hydration [63,64].

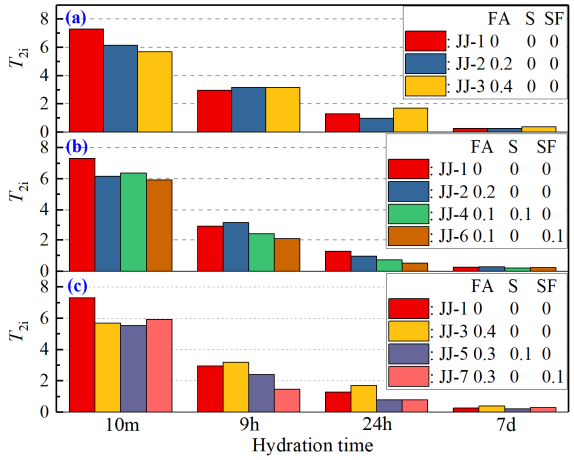


Figure 5. Change of T_{2i} for different cement paste with curing time.

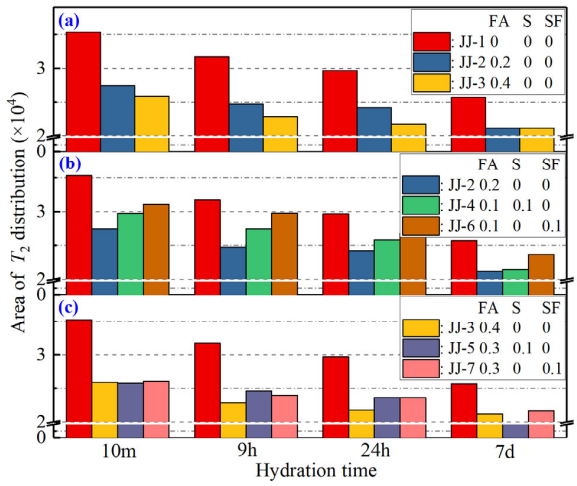
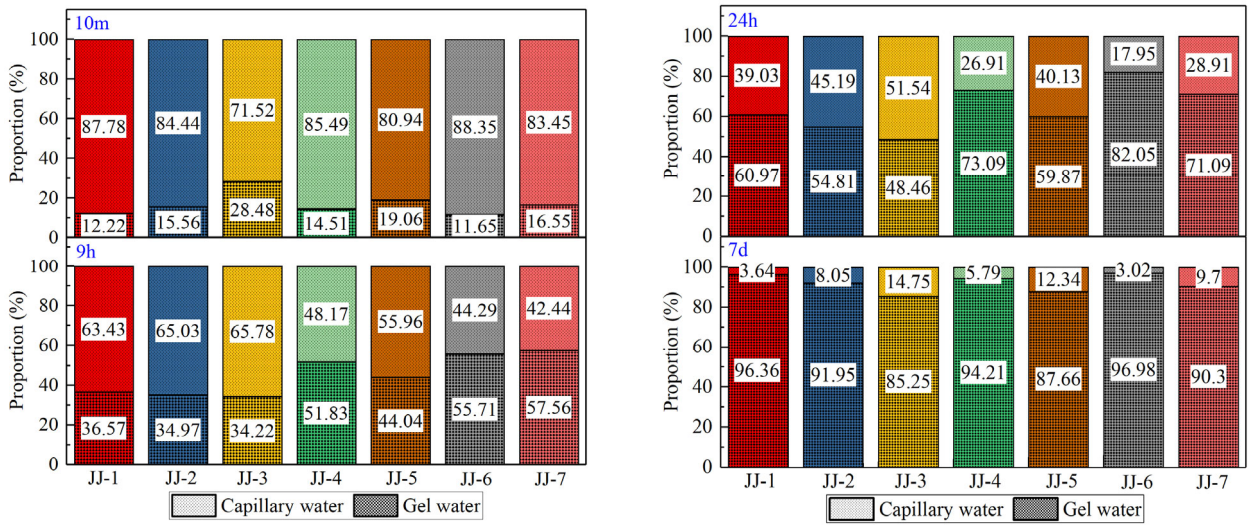


Figure 6. Change of T_2 signal area for different cement paste with curing time.

4.2. Evolution of Evaporable Water

As described above, the distribution of T_2 reflects the motion constraints of liquid water and its content. Because the motion constraints of water in cement-based materials are related to the pore structure, the distribution of T_2 also can be used to describe the pore size and distribution status, as in Equation (2). Li et al. [65] divided the pore formation in hardened cement slurry into four types, including C-S-H interlayer pore, C-S-H gel pore, and small and big capillary pore (between hydration products), and their corresponding values to T_2 are 0.08–0.12 ms, 0.2–0.5 ms, 0.8–1.0 ms, and >10 ms, respectively. Similarly, Scrivener et al. [66] divided the pores corresponding to the three peaks of T_2 distribution into C-S-H interlayer pore, C-S-H gel pore, and capillary pores, and the T_2 times were 0.08–0.12 ms, 0.25–0.5 ms, and >1.0 ms, respectively. Gorce et al. [67] classified pores into gel pores and capillary pores according to T_2 distribution and selected $T_2 = 1.0$ ms as the critical criterion for the two types of pores. In this study, the T_2 distribution at the initial hydration stage of 10 m in Figure 4a shows obvious double peaks on both sides of $T_2 = 1.0$ ms. Combining the above literature research with the results of this study, 1.0 ms is used as the critical T_2 to distinguish gel pores and capillary pores [68], and the water in the two types of pores is divided into gel water and capillary water. Therefore, the proportions of the relaxation signal area of $T_2 < 1.0$ ms and $T_2 \geq 1.0$ ms represent the relative content of gel water and capillary water in the sample, respectively.

Figure 7 presents the evolution of the relative content of gel water and capillary water in the samples with different mix proportions in the curing period. With the increase in curing time, the proportion of gel water has an obvious improvement, and it can reach at least 85% for different contents of the mineral mixture. Meanwhile, the proportion of capillary water gradually decreases to below 15%. At the beginning of hydration (10 min), the evaporable water mainly exists in the form of capillary water. The generation of hydration products and their filling in of large pores leads to pore refinement [15]. So, the evaporable water is gradually distributed in the smaller pores and becomes gel water. Comparing JJ-1, JJ-2, and JJ-3, the proportion of gel water decreases with the increase in FA content at the curing time of 7 days, which means that the addition of FA with a low pozzolanic effect slows down the hydration progress of the FA-C system [9]. Comparing JJ-2, JJ-4, and JJ-6 or JJ-3, JJ-5, and JJ-7, the addition of S and SF also improves the content of gel water, and the order of their influence is SF > S > FA. The reason for this phenomenon is that the activity of SF and S is better than that of FA, and the extremely fine-grained SF (the average particle size is smaller than 0.1 mm) has a better effect on refining pores [13,14].



(**a**) Curing time of 10 m and 9 h (**b**) Curing time of 24 h and 7 days

Figure 7. Evolution of gel water and capillary water relative content.

4.3. Distribution of Pore Structures

Pore structures in cement-based materials can be characterized by converting the T_2 spectral distribution, and the results are displayed in Figure 8. Based on pore classification, these materials contain four types of pores: gel pores (<10 nm), transition pores (10–100 nm), capillary pores (100–1000 nm), and macropores (>1000 nm). It can be seen from Figure 8a that, at the curing time of 10 min, the main pores in samples are capillary pores, and a few are gel pores. With the increase in curing time, the pore size gradually decreases, leading to the increase in gel pores and transition pores, and the decrease in capillary pores. At the curing time of 7 days, the main pores are gel pores and transition pores, and the proportion of the two types of pores is basically equivalent.

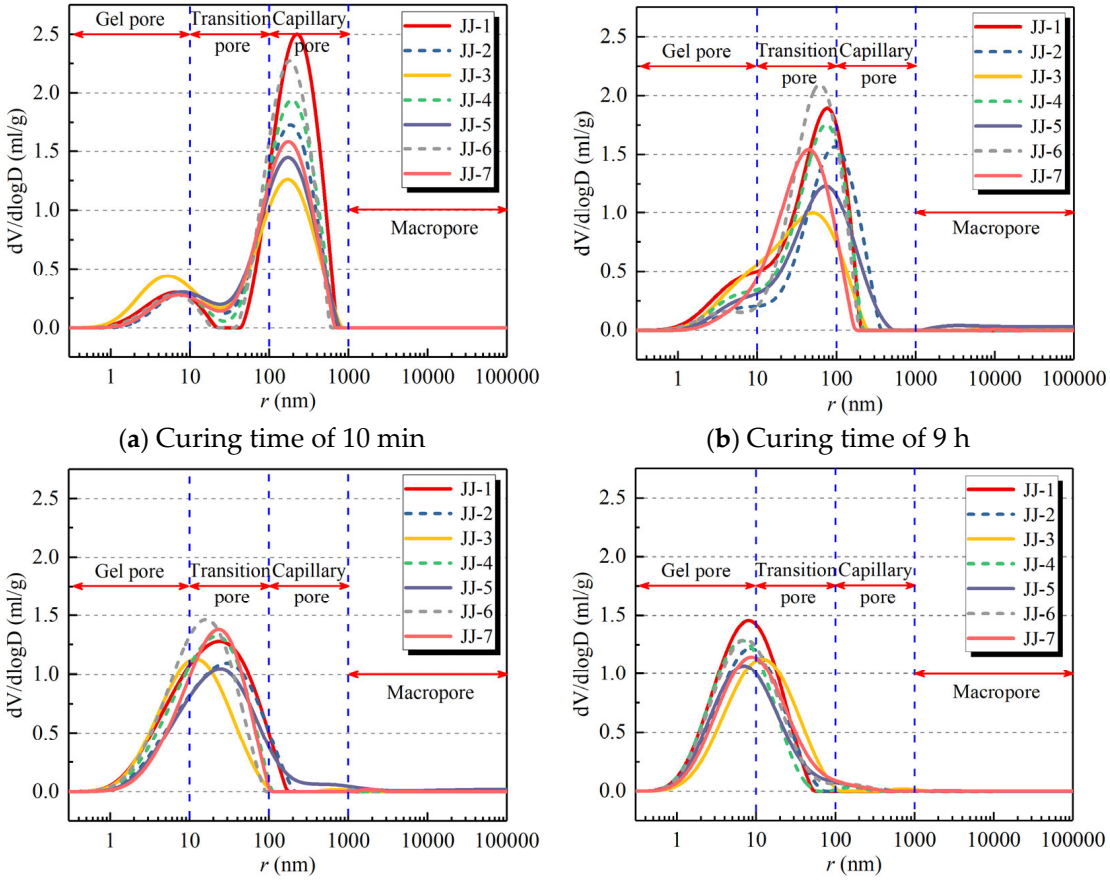


Figure 8. Distribution of pore size in cement paste samples.

Meanwhile, the average porosity of samples with different MAs can be obtained from the distribution of pore size, as presented in Figure 9. It is obvious that the porosity of cement paste gradually decreases with the increase in curing time, and within 10 min–7 days, the porosity is always high. Comparing JJ-1, JJ-2, and JJ-3, the porosity decreases with the increase in FA content in early hydration. Comparing JJ-2, JJ-4, and JJ-6 or JJ-3, JJ-5, and JJ-7, the addition of S and SF in the FA-C system causes an increase in porosity. The reason for the above phenomenon is that, at the curing time of 10 min, the pores are mainly capillary pores. So, the microaggregate effect of FA is the main reason for low porosity [55]. At the curing time of 7 days, the pores are mainly small pores formed in C-S-H gel and generated between gels. The more C-S-H gel, the greater the porosity [69]. So, the porosity of the SF-FA-C system is larger than that of the S-FA-C system, because SF contains higher SiO_2 content to form C-S-H gel. The porosity of the S-FA-C system is larger than that of the

FA-C system, because the low-activity FA basically does not produce C-S-H gel at the early hydration [70].

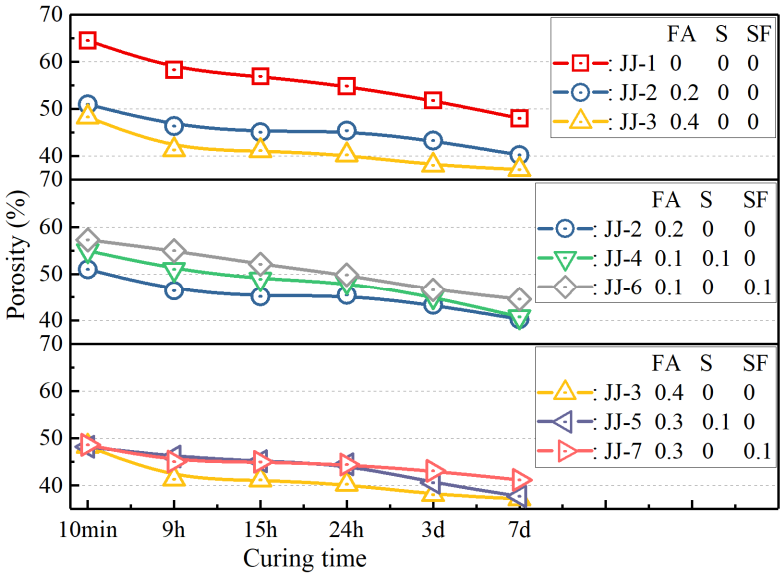
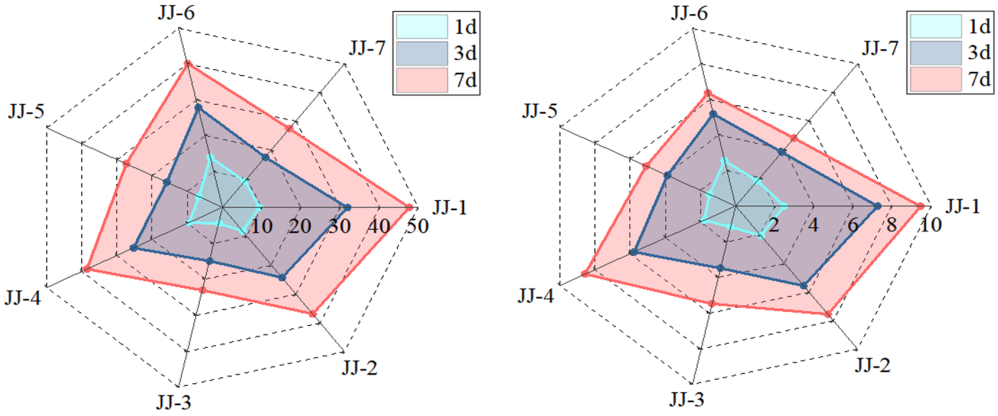


Figure 9. Evolution of porosity with curing time.

4.4. Evolution of Mechanical Property

Besides the evolution of pore structures, the development of early mechanical properties of cement-based materials is also closely related to their hydration progress. Figure 10 presents the evolution of compression strength and flexural strength of cement-based materials with curing time. Comparing Figure 10a,b, for the different samples, the evolution of their compression strengths with curing time is similar to that of flexural strength. Taking compressive strength as an example, it increases with curing time due to the setting and hardening of cement hydration products. At the curing time of 7 days, the compression strength of JJ-1 without any MAs is 47.8 MPa, while that of JJ-2 (with 20% FA) and JJ-3 (with 40% FA) are 37.5 MPa and 23 MPa, respectively. It is caused by the slow reaction rate of FA with low activity. Comparing JJ-2, JJ-4 (with 10% FA and 10% S), and JJ-6 (with 10% FA and 10% SF), their compression strengths are 36.8 MPa, 38.2 MPa, and 40.1 MPa at the curing time of 7 days, and all of them are smaller than that of JJ-1. That is to say, the addition of MAs leads to a decrease in the mechanical properties of cement-based materials at early hydration. Meanwhile, the ranking of minerals' contribution to the early strength of cement-based materials is SF > S > FA. The reason for the above phenomenon is that SF has better activity and can generate denser C-S-H gel [13,14] more quickly, which is helpful for early mechanical properties. However, FA with a low pozzolanic effect hardly contributes to the mechanical properties of cement-based materials within 7 days of hydration [9]. Furthermore, the substitution of FA for cement results in the generation of C-S-H gel and CH, causing the reduction of mechanical properties. Comparing the samples with 40% MAs (JJ-3, JJ-5, and JJ-7) and those with 20% MAs (JJ-2, JJ-3, and JJ-6), the evolution of their compression strengths also verified the above viewpoint that the greater the MA content, the lower the early strength. Specifically, the activity of MA is lower than that of cement, so the addition (substitution) of more MA leads to fewer hydration products in a solidified state in the early stage of hydration to contribute to the early strength. In addition, the evolution of the compressive strength of cement-based materials with MA is presented in Figure 11. It is consistent with that of porosity at the early hydration stage, and the two are basically in a linear relationship.



(**a**) Compression strength (MPa) (**b**) Flexural Strength (MPa)

Figure 10. Evolution of early mechanical properties of cement-based materials with curing time.

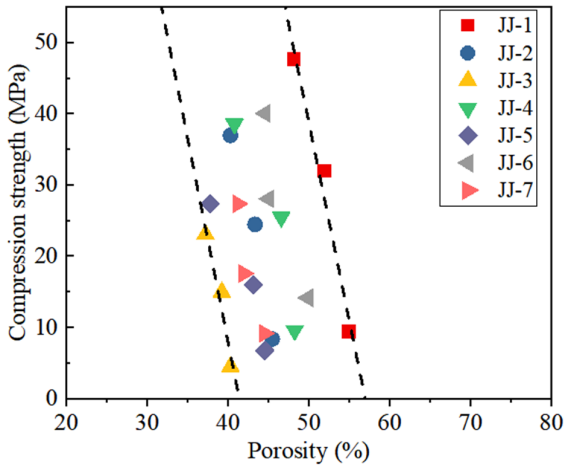


Figure 11. Relationship between porosity and compression strength of cement-based materials.

5. Conclusions

(1) At the beginning of hydration (10 min), T_2 distribution presents double peaks (an obvious main peak and a weak peak), and the relaxation time of the main peak is about 1~10 ms. With the curing time, the distribution of the relaxation peak shows a trend of gradually changing to a single main peak. At the curing time of 24 h, the relaxation time of the single main peak is about 0.1~1 ms.

(2) T_{2i} (relaxation time of the main peak) reflects the motion characteristics of water molecules. At the early hydration stage (within 24 h), T_{2i} has a rapid decrease and then gradually stabilizes. It is because the formation of hydration products refines larger pores, causing the evaporated water to be distributed in smaller pores with more motion constraints. However, the difference in T_{2i} of different mix proportions is not significant, indicating that the type and content of MA have little effect.

(3) The relaxation signal area reflects the content of unreacted evaporated water in samples, including the gel water and capillary water. So, the results of the relaxation signal area evolution show that the total content of water consumed by the hydration reaction decreases, and the proportion of gel water obviously increases, while that of capillary water gradually decreases. For MAs, the gel water content decreases with the increase in FA content, and the addition of S and SF also improves the gel water content, and the order of their influence is SF > S > FA.

(4) At a curing time of 10 mins, the main pores are capillary pores. With the curing time, the pore size also gradually decreases, leading to an increase in gel pores and transition pores. At 7 days, the main pores are gel pores. Meanwhile, the porosity also

decreases with curing time, i.e., without MA, it decreases from 64.8% at 10 mins to 48% at 7 days. With the effect of MA, the porosity of the FA-C (cement) system decreases with the increase in FA content. The addition of S and SF in the FA-C system causes the porosity to increase, and the order of their porosity is SF-FA-C system > S-FA-C system > FA-C system.

(5) The ranking of the MA contribution to the early strength is SF > S > FA, but significantly lower than cement itself, i.e., the compression strength at the curing time of 7 days is 47.8 MPa for 0%MA, 40.1 MPa for 10%FA + 10%SF, 38.6 MPa for 10%FA + 10%S, and 37 MPa for 20%FA. It indicates that adding multiple types of MA is an effective method to improve early strength while ensuring other performance.

Author Contributions: Conceptualization, G.-J.Y.; methodology, L.M.; software, Z.-Q.S.; formal analysis, Z.-Y.Z.; investigation, S.-S.W.; resources, Y.-J.T.; writing—original draft preparation, Y.-J.T.; writing—review and editing, G.-J.Y.; funding acquisition, G.-J.Y. and Y.-J.T. All authors have read and agreed to the published version of the manuscript.

Funding: This study is supported by the Natural Science Foundation of China (52308262), the Natural Science Foundation of the Jiangsu Higher Education Institutions of China (20KJB430030), the "Chunhui Plan" collaborative research project of the Ministry of Education (HZKY20220199), the Zhejiang Provincial Natural Science Foundation of China (LQ21E080008), the Ningbo Natural Science Foundation (2023J176), the Qing Lan Project, the Yangzhou "Lv-yang-jin-feng" project, and the Scientific Research Start-up Foundation of Ningbo University of Technology in 2020.

Data Availability Statement: We can provide all research data through email as long as the authors required it.

Acknowledgments: Thanks to Cheng Shanshan for her guidance in analyzing the results.

Conflicts of Interest: The authors declare no conflict of interest.

References

1. Scrivener, K.L.; Juilland, P.; Monteiro, P.J. Advances in understanding hydration of Portland cement. *Cem. Concr. Res.* **2015**, *78*, 38–56. [CrossRef]
2. Izadifar, M.; Natzeck, C.; Emmerich, K.; Weidler, P.G.; Gohari, S.; Burvill, C.; Thissen, P. Unexpected Chemical Activity of a Mineral Surface: The Role of Crystal Water in Tobermorite. *J. Phys. Chem.* **2022**, *126*, 12405–12412. [CrossRef]
3. Izadifar, M.; Königer, F.; Gerdes, A.; Woll, C.; Thissen, P. Correlation between composition and mechanical properties of calcium-silicate-hydrates identified by infrared spectroscopy and density functional theory. *J. Phys. Chem.* **2019**, *123*, 10868–10873. [CrossRef]
4. Scrivener, K.L.; Nonat, A. Hydration of cementitious materials, present and future. *Cem. Concr. Res.* **2011**, *41*, 651–665. [CrossRef]
5. She, A.M.; Ma, K.; Wang, Z.P.; Yao, W. Characterization of hardened cement paste pore structure by low field NMR cryoporometry. *J. Build. Mater.* **2021**, *24*, 916–920.
6. Sun, Y.; Wang, Z.H.; Park, D.J.; Kim, W.S.; Kim, H.S.; Yan, S.R.; Lee, H.S. Analysis of the isothermal hydration heat of cement paste containing mechanically activated fly ash. *Thermochim. Acta* **2022**, *715*, 179273. [CrossRef]
7. Nedunuri, S.S.S.A.; Sertse, S.G.; Muhammad, S. Microstructural study of Portland cement partially replaced with fly ash, ground granulated blast furnace slag and silica fume as determined by pozzolanic activity. *Constr. Build. Mater.* **2020**, *238*, 117561. [CrossRef]
8. Kooshafar, M.; Madani, H. An investigation on the influence of nano silica morphology on the characteristics of cement composites. *J. Build. Eng.* **2020**, *30*, 101293. [CrossRef]
9. Zeng, Q.; Li, K. Reaction and microstructure of cement-fly-ash system. *Mater. Struct.* **2015**, *48*, 1703–1716. [CrossRef]
10. Sun, Y.; Lee, H.S. Using ensemble model to predict isothermal hydration heat of fly ash cement paste considering fly ash content, water to binder ratio and curing temperature. *Case Stud. Constr. Mater.* **2023**, *18*, e01984. [CrossRef]
11. Giergiczny, Z. Fly ash and slag. *Cem. Concr. Res.* **2019**, *124*, 105826. [CrossRef]
12. Naik, T.R.; Singh, S.S.; Hossain, M.M. Permeability of concrete containing large amounts of fly ash. *Cem. Concr. Res.* **1994**, *24*, 913–922. [CrossRef]
13. Cai, Y.M.; Hou, P.K.; Cheng, X.; Du, P.; Ye, Z.M. The effect of nanoSiO_2 on the properties of fresh and hardened cement-based materials through its dispersion with silica fume. *Constr. Build. Mater.* **2017**, *148*, 770–780. [CrossRef]
14. Nguyen, V.T.; Lee, S.Y.; Chung, S.Y.; Moon, J.H.; Kim, D.J. Use of multiphase voxels to simulate the effects of nano-silica on cement hydration. *Case Stud. Constr. Mater.* **2023**, *18*, e01909. [CrossRef]
15. Qu, L.; Song, W.H.; Wang, Q.; Xu, S.S.; Hou, C. Effects of hydrophobic modified fly ash on resistance of chloride corrosion and water penetration of cement mortar in the early hydration stage. *J. Build. Eng.* **2023**, *64*, 105573. [CrossRef]

16. Wang, H.; Wu, D.; Mei, Z. Effect of fly ash and limestone powder on inhibiting alkali aggregate reaction of concrete. *Constr. Build. Mater.* **2019**, *210*, 620–626. [CrossRef]
17. He, P.P.; Drissi, S.; Hu, X.; Liu, J.H.; Shi, C.J. Investigation on the influential mechanism of FA and GGBS on the properties of CO2-cured cement paste. *Cem. Concr. Compos.* **2023**, *142*, 105186. [CrossRef]
18. Liu, Z.; Takasu, K.; Koyamad, H.; Suyama, H. A study on engineering properties and environmental impact of sustainable concrete with fly ash or GGBS. *Constr. Build. Mater.* **2022**, *316*, 125776. [CrossRef]
19. Das, P.; Chakraborty, S.; Dubey, B.; Barai, S.V.; Cheela, V.R.S.; Mistri, A. Performance assessment and life cycle analysis of concrete containing ferrochrome slag and fly ash as replacement materials—A circular approach. *Constr. Build. Mater.* **2022**, *347*, 128609. [CrossRef]
20. Nguyen, V.M.; Phung, T.B.; Pham, D.T.; Ho, L.S. Mechanical properties and durability of concrete containing coal mine waste rock, F-class fly ash, and nano-silica for sustainable development. *J. Eng. Res.* **2023**, *in press*. [CrossRef]
21. Kumar, M.H.; Saikrishnamacharyulu, I.; Mohanta, N.R.; Ashutosh, A.; Mishra, P.; Smantaray, S. Mechanical behaviour of high strength concrete modified with triple blend of fly ash, silica fume and steel fibers. *Mater. Today Proc.* **2022**, *65*, 933–942. [CrossRef]
22. Huseien, G.F.; Khamehchi, M.; Kubba, Z.; Benjeddou, O.; Mahmoodi, M.J. Freeze-thaw cycle and abrasion resistance of alkali-activated FA and POFA-based mortars: Role of high volume GBFS incorporation. *Heliyon* **2023**, *9*, e17672. [CrossRef] [PubMed]
23. Hasan, M.F.; Hassan, M.A.; Lateef, K.H. Effect of MK and SF on the concrete mechanical properties. *Mater. Today Proc.* **2021**, *42*, 2914–2919. [CrossRef]
24. Shamass, R.; Rispoli, O.; Limbachiya, V.; Kovacs, R. Mechanical and GWP assessment of concrete using Blast Furnace Slag, Silica Fume and recycled aggregate. *Case Stud. Constr. Mater.* **2023**, *18*, e02164. [CrossRef]
25. Sahoo, S.; Parhi, P.K.; Panda, B.C. Durability properties of concrete with silica fume and rice husk ash. *Clean. Eng. Technol.* **2021**, *2*, 100067. [CrossRef]
26. Amin, M.N.; Rehman, K.U.; Shahzada, K.; Khan, K.; Wahab, N.; Alabdullah, A.A. Mechanical and microstructure performance and global warming potential of blended concrete containing rice husk ash and silica fume. *Constr. Build. Mater.* **2022**, *346*, 128470. [CrossRef]
27. Paithankar, D.; Sharma, A.; Thenmozhi, S.; Ramteke, P.; Dhanalakshmi, A.; Sivakumar, S. Influence of glass powder silica fume and scrapped ceramic waste on the mechanical properties of concrete. *Mater. Today Proc.* **2023**, *in press*. [CrossRef]
28. Amin, M.; Zeyad, A.M.; Tayeh, B.A.; Agwa, I.S. Effect of ferrosilicon and silica fume on mechanical, durability, and microstructure characteristics of ultra high-performance concrete. *Constr. Build. Mater.* **2022**, *320*, 126233. [CrossRef]
29. Linderoth, O.; Wadsö, L.; Jansen, D. Long-term cement-hydration studies with isothermal calorimetry. *Cem. Concr. Res.* **2021**, *141*, 106344. [CrossRef]
30. Han, F.; Zhang, Z.; Wang, D.; Yan, P. Hydration heat evolution and kinetics of blended cement containing steel slag at different temperatures. *Thermochim. Acta* **2015**, *605*, 43–51. [CrossRef]
31. Garcia, E. Nonevaporable water from neat OPC and replacement materials in composite cement hydrated at different temperatures. *Cem. Concr. Res.* **2003**, *33*, 1883–1888. [CrossRef]
32. Chu, D.C.; Kleib, J.; Amar, M.; Benzerzour, M.; Abriak, N. Determination of the degree of hydration of Portland cement using three different approaches: Scanning electron microscopy (SEM-BSE) and Thermogravimetric analysis (TGA). *Case Stud. Constr. Mater.* **2021**, *15*, e00754. [CrossRef]
33. Scrivener, K.; Ouzia, A.; Juilland, P.; Mohamed, A.K. Advances in understanding cement hydration mechanisms. *Cem. Concr. Res.* **2019**, *124*, 105823. [CrossRef]
34. Krstulović, R.; Dabić, P.A. Conceptual model of the cement hydration process. *Cem. Concr. Res.* **2000**, *30*, 693–698. [CrossRef]
35. Pane, I.; Hansen, W. Investigation of blended cement hydration by isothermal calorimetry and thermal analysis. *Cem. Concr. Res.* **2005**, *35*, 1155–1164. [CrossRef]
36. Zhao, K.Y.; Zhang, P.; Kong, X.M.; Li, H.X.; Zhao, H.T. Recent progress on Portland cement hydration kinetic models and experimental methods. *J. Chin. Ceram. Soc.* **2022**, *50*, 1728–1761.
37. Li, Z.J.; Wei, X.S.; Li, W.L. Preliminary interpretation of hydration process of Portland cement using resistivity measurement. *ACI Mater. J.* **2003**, *100*, 253–257.
38. Yim, H.J.; Bae, Y.H.; Jun, T.B. Hydration and microstructural characterization of early-age cement paste with ultrasonic wave velocity and electrical resistivity measurements. *Constr. Build. Mater.* **2021**, *303*, 124508. [CrossRef]
39. Xu, D.Y.; Chen, H.C.; Hu, Y.; Sun, D.D.; Du, P.; Liu, P. Ultrasonic monitoring and property prediction of cement hydration with novel omnidirectional piezoelectric ultrasonic transducer. *J. Build. Eng.* **2023**, *72*, 106612. [CrossRef]
40. Zhang, J.; Qin, L.; Li, Z.J. Hydration monitoring of cement-based materials with resistivity and ultrasonic methods. *Mater. Struct.* **2009**, *42*, 15–24. [CrossRef]
41. Xu, W.B.; Li, Q.B.; Hu, Y. Water content variations in the process of concrete setting. *J. Hydraul Eng.* **2017**, *36*, 92–103.
42. Li, C.J.; Sun, Z.P.; Li, Q.; Luo, Q. Application of low-field nuclear magnetic resonance in cement-based materials. *Mater. Rev.* **2016**, *30*, 133–138.
43. Gajewicz, A.M.; Gartiner, E.; Kang, K.; Mcdonald, P.J.; Yermakou, V. A ^{1}H NMR relaxometry investigation of gel–pore drying shrinkage in cement pastes. *Cem. Concr. Res.* **2016**, *86*, 12–19. [CrossRef]
44. Cohen, M.H.; Mendelson, K.S. Nuclear magnetic relaxation and the internal geometry of sedimentary rocks. *J. Appl. Phys.* **1982**, *53*, 1127–1135. [CrossRef]

45. Valori, A.; McDonald, P.J.; Scrivener, K.L. The morphology of C-S-H lessons from H-1 nuclear magnetic resonance relaxometry. *Cem. Concr. Res.* **2013**, *49*, 65–81. [CrossRef]
46. Zhao, H.T.; Wu, X.; Huang, Y.Y.; Zhang, P.; Tian, Q.; Liu, J.P. Investigation of moisture transport in cement-based materials using low-field nuclear magnetic response imaging. *Mag. Concr. Res.* **2021**, *73*, 252–270. [CrossRef]
47. Zhang, A.; Ge, Y. 1H Low Field NMR relaxation characteristics of hydration process of while cement modified with silica nanoparticles. *J. Chin. Ceram. Soc.* **2021**, *49*, 1662–1669.
48. Liu, H.; Sun, Z.P.; Yang, J.B.; Ji, Y.L. A novel method for semi-quantitative analysis of hydration degree of cement by 1H low-field NMR. *Cem. Concr. Res.* **2021**, *141*, 106329. [CrossRef]
49. Ji, Y.L.; Sun, Z.P.; Yang, X.; Li, C.J.; Tang, X.B. Assessment and mechanism study of bleeding process in cement paste by 1H low-field NMR. *Constr. Build. Mater.* **2015**, *100*, 255–261. [CrossRef]
50. Zhao, H.T.; Jiang, K.D.; Di, Y.F.; Xu, W.; Li, W.; Tian, Q.; Liu, J.P. Effects of curing temperature and superabsorbent polymers on hydration of early-age cement paste containing a CaO-based expansive additive. *Mater. Struct.* **2019**, *52*, 108. [CrossRef]
51. Zhao, H.T.; Ding, J.; Huang, Y.Y.; Tang, Y.M.; Xu, W.; Huang, D.H. Experimental analysis on the relationship between pore structure and capillary water absorption characteristics of cement-based materials. *Struct. Concr.* **2019**, *20*, 1750–1762. [CrossRef]
52. Brownstein, K.R.; Tarr, C.E. Importance of classical diffusion in NMR studies of water in biological cells. *Phys. Rev. A* **1979**, *19*, 2446–2453. [CrossRef]
53. Song, Y.Q. Magnetic resonance of porous media (MRPM): A perspective. *J. Magn. Reson.* **2013**, *229*, 12–24. [CrossRef] [PubMed]
54. Muller, A.C.A.; Scrivener, K.L.; Gajewicz, A.M.; McDonald, P.J. Densification of C-S-H measured by ^{1}H NMR relaxometry. *J. Phys. Chem. C* **2013**, *117*, 403–412. [CrossRef]
55. Fu, J.X.; Wang, K.; Wang, J. Internal pore evolution and early hydration characterization of fly ash cement backfill. *J. Build. Eng.* **2023**, *72*, 106716. [CrossRef]
56. Juenger, M.C.G.; Jennings, H.M. Examining the relationship between the microstructure of calcium silicate hydrate and drying shrinkage of cement pastes. *Cem. Concr. Res.* **2002**, *32*, 289–296. [CrossRef]
57. Poli, T.; Toniolo, L.; Valentini, M.; Bizzaro, G.; Melzi, R.; Tedoldi, F.; Cannazza, G. A portable NMR device for the evaluation of water presence in building materials. *J. Cult. Herit.* **2007**, *8*, 134–140. [CrossRef]
58. Bertram, H.C.; Jandersen, H.; Karlsson, A.H. Comparative study of low-field NMR relaxation measurements and two traditional methods in the determination of water holding capacity of pork. *Meat Sci.* **2001**, *57*, 125–132. [CrossRef]
59. Liu, L.; He, Z.; Cai, X.; Fu, S.J. Application of low-field NMR to the pore structure of concrete. *Appl. Magn. Reson.* **2021**, *52*, 15–31. [CrossRef]
60. Wang, Y.; Burris, L.; Hooton, R.D.; Shearer, C.R.; Suraneni, P. Effects of unconventional fly ashes on cementitious paste properties. *Cem. Concr. Compos.* **2022**, *125*, 104291. [CrossRef]
61. Pipikaki, P.; Katsioti, M. Study of the hydration process of quaternary blended cements and durability of the produced mortars and concretes. *Constr. Build. Mater.* **2009**, *23*, 2246–2250. [CrossRef]
62. Wen, X.D.; Yin, G.J.; Xia, L.; Zhou, M.; Feng, L.; Wu, J.Y. Spatiotemporal evolution of water and pore structure in cement-based materials containing SRA by LF NMR. *Mater. Today Commun.* **2023**, *35*, 106076.
63. Xu, Z.H.; Guo, Z.H.; Zhao, Y.S. Hydration of blended cement with high-volume slag and nano-silica. *J. Build. Eng.* **2023**, *64*, 105657. [CrossRef]
64. Whittaker, M.; Zajac, M.; Haha, M.B.; Bullerjahn, F.; Black, L. The role of the alumina content of slag, plus the presence of additional sulfate on the hydration and microstructure of Portland cement-slag blends. *Cem. Concr. Res.* **2014**, *66*, 91–101. [CrossRef]
65. Li, W.Y.; Yin, J.H.; Wang, J.; Yang, H.J.; Kong, X.M. Principles and applications of low-field nuclear magnetic resonance in cementitious materials. *J. Chin. Ceram. Soc.* **2022**, *50*, 2992–3008.
66. Scrivener, K.; Snellings, R.; Lothenbach, B. *A Practical Guide to Microstructural Analysis of Cementitious Materials*; Science Press: Beijing, China, 2021.
67. Gorce, J.P.; Milstone, N.B. Probing the microstructure and water in composite cement blends. *Cem. Concr. Res.* **2007**, *37*, 310–318. [CrossRef]
68. Faure, P.; Care, S.; Magat, J.; Chaussadent, T. Drying effect on cement paste porosity at early age observed by NMR methods. *Constr. Build. Mater.* **2012**, *29*, 496–503. [CrossRef]
69. Wu, F.F.; Shi, K.B.; Dong, S.K.; Chen, S.S.; Ci, J.; Wang, X.; Zhang, K. Influence of admixture and water-cement ratio on hydration products and mechanical properties of cement-based materials. *Trans. Chin. Soc. Agric. Eng.* **2016**, *32*, 119–126.
70. Golewski, G.L. The role of pozzolanic activity of siliceous fly ash in the formation of the structure of sustainable cementitious composites. *Sustain. Chem.* **2022**, *3*, 520–534. [CrossRef]

Disclaimer/Publisher's Note: The statements, opinions and data contained in all publications are solely those of the individual author(s) and contributor(s) and not of MDPI and/or the editor(s). MDPI and/or the editor(s) disclaim responsibility for any injury to people or property resulting from any ideas, methods, instructions or products referred to in the content.